LETTER

Is Porosity at the MOF/Polymer Interface Necessarily an Obstacle to Optimal Gas-Separation Performances in Mixed Matrix Membranes?

Dong Fan,[§] Aydin Ozcan,[§] Naseem A. Ramsahye, Dan Zhao, Guillaume Maurin, and Rocio Semino*

Read Online

ACCESS | Metrics & More | Article Recommendations | SI Supporting Information

ABSTRACT: Current MOF/polymer mixed matrix membranes (MMMs) design relies on the assumption that it is necessary to avoid interfacial porosity in order to achieve high-level gas-separation performances, but is this assumption valid in all cases, for all separation mechanisms? This communication proves that this is not always true by considering NUS-8/PIM-1, a prototypical MMM for CO_2 capture. Our molecular simulations approach integrating quantum calculations, force field-based Monte Carlo, and equilibrium/non-equilibrium molecular dynamics simulations, revealed that a porosity generated at the NUS-8/PIM-1 interface in the form of microvoids favors the interactions between CO_2 and the NUS-8 surface and therefore contributes to ensure a high CO_2/N_2 and CO_2/CH_4 selectivity for the corresponding MMM, preserving the pure NUS-8 membrane value and exhibiting a high flux for CO_2. This high-level performance is achieved by means of a solubility-driven separation mechanism, as opposed to previously studied diffusion-driven separations where the interface porosity had been shown to deteriorate the MMM separation performance. We believe that these results will change the current paradigm in the field of MOF/polymer MMMs, paving the way toward new strategies for the development of highly efficient membranes for gas separation.
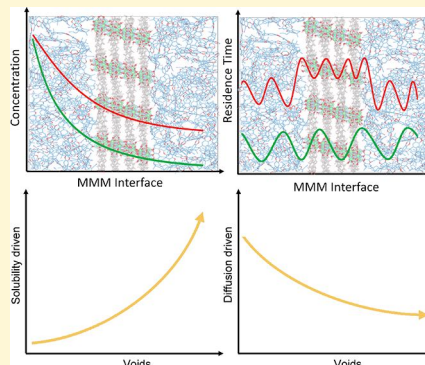
High flux and highly selective membranes have been largely sought after over the last decades for achieving industrially and environmentally relevant energy-efficient separations in gas and liquid phases.[1−4] Notably, mixed matrix membranes (MMMs) have emerged as next-generation gas-separation membranes by combining the benefits of solution processable polymer matrices with the unique tunable adsorptive and diffusive properties of diverse fillers.[5−8] In particular, metal−organic framework (MOF)/polymer MMMs have been shown to largely overcome the well-known trade-off between permeability and selectivity that prevails in current polymer-based membranes in the field of gas separation.[9−13]

In this context, there is a wealth of work covering the fabrication of MOF/polymer-based continuous films, with high MOF loading and homogeneous dispersion into the polymer matrices.[10,12,14−16] Many other experimental studies have instead focused on testing MMMs' performances for a range of gas mixture separations of utmost importance in the fields of natural gas upgrading and hydrocarbon recovery, regardless of their MOF contents and the MOF/polymer affinity (also called compatibility).[6,17−19] Meanwhile, the key microscopic

parameters that control the onset of a good MOF/polymer compatibility have been identified thanks to the study of the interface structure of a series of MOF/polymer composites by computer simulations.[20,21] In contrast, the microscopic origin of the MMMs' performances has not yet been unveiled, and in particular, the role of the MOF/polymer interface structure has not yet been determined.

New porosities emerging at many MMMs' interfaces in the form of microvoids or gaps have been evoked to play a negative impact on their gas-separation performances because of a nonselective increase of permeability.[22,23] This has led to speculation that there is a link between MOF/polymer compatibility and the gas-separation performance of the resulting MMM. However, a good compatibility, i.e., the
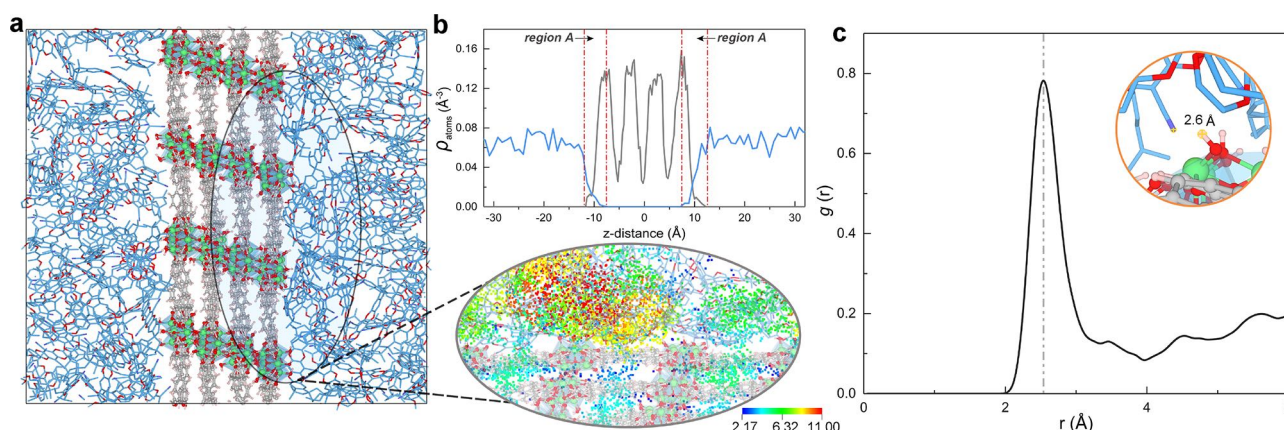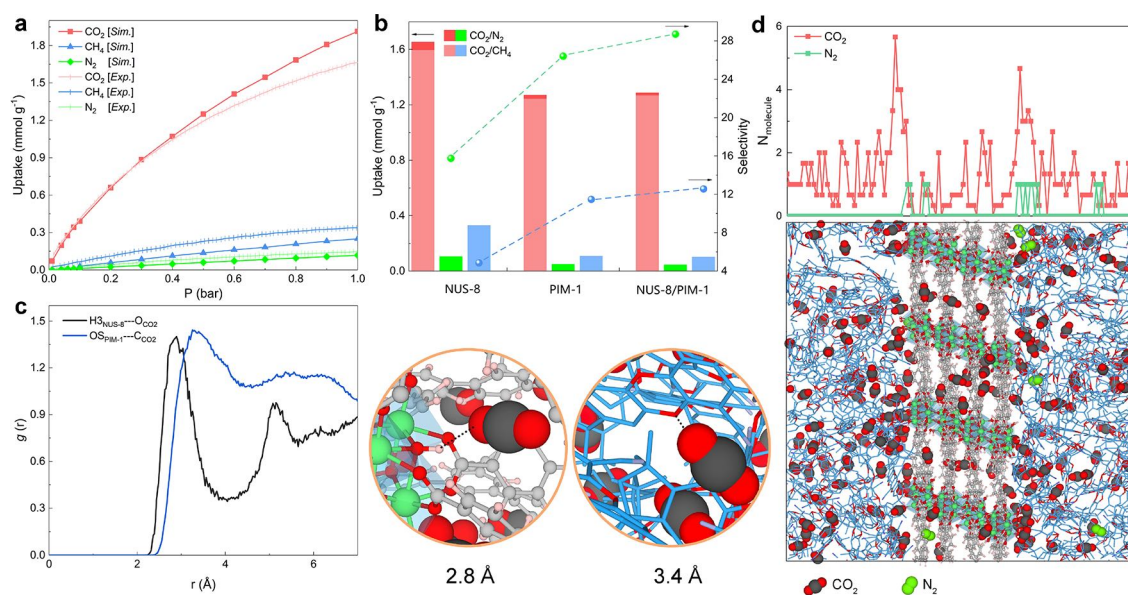
Figure 1. Structure of the NUS-8/PIM-1 composite. (a) Representative snapshot of the NUS-8/PIM-1 atomistic model. Color scheme: PIM-1, blue wireframe; Zr, green; O, red; H, pink; C, gray, with a zoom-in of the corresponding 3D pore size distribution for the flexible NUS-8/PIM-1 interface, with the pore diameter (in Å) colored according to the legend. (b) Atomic density plot of PIM-1 and NUS-8 as a function of the z-coordinate for a representative configuration of the NUS-8/PIM-1 composite (the region delimited by red dashed lines indicates *region A*). (c) Radial distribution function between H_{NUS-8} (−OH) and N_{PIM-1} in the NUS-8/PIM-1 composite. The corresponding interaction is illustrated in the inset.

absence of surface porosities, does not necessarily translate into a high-level separation performance. For instance, polymer penetration into the MOF pores can result in thus pore blockage,[20,24] which was suggested as a possible explanation of the low permeability measured experimentally for highly compatible MOF/polymer MMMs. An open question still remains: is porosity at MOF/polymer interfaces necessarily an obstacle to optimal gas-separation performances in MMMs? This gap in knowledge comes from the fact that investigations on this topic at the atomistic level are still very scarce.[25−27] Indeed, computational studies in this field have focused to date on numerical simulations of MMMs' gas-separation performances via the use of mathematical models (such as Maxwell, Felske, or Lewis−Nielsen models). To the best of our knowledge, the only attempt to explore the influence of the structure and dynamic modes of the MOF/polymer interface in gas transport through an MMM in real membrane operation conditions has been made very recently.[28] Non-equilibrium molecular dynamics (NEMD) simulations were applied to model the transport properties of guests in a ZIF-8/Polymer of Intrinsic Microporosity 1 (PIM-1) MMM based on a realistic atomistic description of the composite and its interface to study the H_2/CH_4 mixture separation. In this latter work, microscopic voids were detected at the MOF/polymer interface and they were proposed as the origin of a reduction of the selectivity of the composite with respect to its pure component counterparts.

Herein, we explore adsorption/separation and transport properties of a MOF/polymer composite for some of the most challenging gas-separation processes by means of an integrated molecular simulation approach. As a proof-of-concept, we have selected the NUS-8/PIM-1 MMM system that has very recently been reported as an excellent candidate for CO_2 capture with outstanding separation performances in pre- (CO_2/CH_4) and post-combustion (CO_2/N_2) conditions.[29] Density functional theory (DFT) calculations and flexible force field-based molecular dynamics (MD) simulations were first combined to build an atomistic model for the composite. The interfacial region formed between the two components was analyzed and new porosities in the form of microvoids were detected. Monte Carlo simulations were further conducted to

compute the thermodynamic single component and mixture adsorption properties of the resulting composite. A reasonable agreement between the simulated and experimentally measured adsorption isotherms was found, thus validating the atomistic structure model for the NUS-8/PIM-1 composite. The analysis of the microscopic adsorption mechanism further revealed that the presence of the interfacial microvoids does not alter the high thermodynamic separation performance of the MMM for CO_2 over both CH_4 and N_2. Finally, the gas permeability and selectivity of the composite were explored by means of non-equilibrium concentration-gradient-driven molecular dynamics (CGD-MD) simulations.[30] The conclusions drawn from this study are expected to enhance our understanding of the role played by the interfaces on the separation performances of MMMs driven either by solubility or diffusion. In particular, we demonstrate that the presence of voids at the MOF/polymer interface does not have a negative impact on the performance of MMMs for solubility-driven separations, and thus, the speculated compatibility/performance link need not be taken for granted.

The NUS-8/PIM-1 composite model was built by applying a computational approach integrating quantum- and force field-based simulations that we previously developed and applied to study MOF/polymer compatibility for several composites.[20,31] NUS-8(Zr) can be described by stacked monolayers containing 3-connected 1,3,5-benzenetribenzoate (BTB) linked by 6-coordinated $Zr_6(OH)_4O_4$ inorganic nodes.[32] This two-dimensional (2D) nanosheet MOF exhibits unidirectional diamond shaped channels of 6 Å diameter that ensure an efficient transport of CO_2.[29] Three surface slab models of this 2D nanosheet MOF exhibiting different stacking configurations were created and geometry optimized at the DFT level using the CP2K software.[33,34] The AA stacking configuration of the bulk MOF along the (001) plane was selected by taking into account both lowest energy and better agreement with the experimentally measured cell parameters. The surface was terminated considering the dissociative adsorption of water molecules, since the NUS-8 synthesis was carried out in aqueous solution. This results in −OH terminations at the external part of the surface: Zr atoms are capped by −OH functions, and −H is added to an oxygen atom at the organic

Figure 2. Gas adsorption properties of the NUS-8/PIM-1 composite. (a) Comparison of the GCMC-simulated and experimental CO_2, N_2, and CH_4 single-component adsorption isotherms for the NUS-8/PIM-1 composite at 298 K. (b) CO_2, N_2, and CH_4 uptake capacity and thermodynamic selectivity of pure NUS-8, pure PIM-1, and the NUS-8/PIM-1 composite for the equimolar CO_2/N_2 and CO_2/CH_4 mixtures adsorption isotherms at 298 K and a total pressure of 1 bar. (c) RDFs corresponding to the most prominent interactions between CO_2 and the NUS-8/PIM-1 composite in the case of the CO_2/N_2 mixture at 1 bar and illustration of the preferential site-to-site interactions between CO_2 and each component of the NUS-8/PIM-1 composite. (d) Number of N_2 and CO_2 molecules along the direction perpendicular to the MMM for the coadsorption of CO_2/N_2 in the NUS-8/PIM-1 composite at total pressure of 1 bar and 298 K and the corresponding GCMC snapshot. The color scheme for all snapshots is the same as in Figure 1.

---

linker at the surface as done previously for UiO-66.[20] An illustration of the MOF surface model is provided in Figure S1. This model was then combined with a PIM-1 model created in silico as implemented in the *Polymatic* package.[35] The resulting composite model was subsequently equilibrated by a series of MD simulations in the *NVT* and the *NP$_z$T* ensembles, where P_z corresponds to the pressure component in the *z* direction, that is, the direction perpendicular to the MOF surface slab. These MD simulations were performed using a modified version of the DL_POLY Classic code (2.18).[36] The final dimensions of the equilibrated models are 40.39 × 70.10 × 67.74 Å^3. The polymer component has a thickness of about 50 Å, thick enough in the *z* direction to avoid interactions between the periodic images of the NUS-8 surface. The two components were treated as fully flexible, based on the UFF,[37] GAFF,[38] and TraPPE[39] force fields. The MOF and polymer force field parameters were preliminarily validated by reproducing some structural features of the bulk pure components, while the MOF/polymer nonbonded interactions were described by the sum of a 12−6 Lennard-Jones potential term and a Coulombic contribution. Partial charges for the atoms were obtained from DFT calculations, and the Lennard-Jones crossed terms were computed using the Lorentz−Berthelot mixing rules. Further details on the construction and geometry optimization of the MOF surface model, polymer, and composite, as well as the validation of the flexible force field parameters for NUS-8, are provided in the Supporting Information (see Figures S1−S5 and Tables S1−S6).

Grand Canonical Monte Carlo (GCMC) simulations were performed on the resulting NUS-8/PIM-1 composite to assess its CO_2, CH_4, and N_2 single-component and binary mixtures (CO_2/N_2 and CO_2/CH_4) thermodynamic adsorption properties using the RASPA code.[40] Predictions of the gas transport through the composite for the two binary mixtures were further carried out by CGD-MD simulations[30] using the GROMACS-2019.4 package[41] patched with a modified PLUMED-2 enhanced sampling plug-in.[42] All details and parameters for the GCMC and CGD-MD simulations are provided in the SI.

A representative snapshot of the NUS-8/PIM-1 composite model is illustrated in Figure 1a. The NUS-8 nanosheet is located at the middle of the simulation box, surrounded by the PIM-1 polymer on both sides. Figure 1b shows the atomic density profile of the NUS-8/PIM-1 composite as a function of the z direction. The atomic density of PIM-1 oscillates around a constant value while far from the NUS-8 surface (*region B*) and decays to zero at the close proximity of it (*region A*, the onset of the interface). There is no evidence of polymer penetration into the porosity of the NUS-8 structure. However, there is MOF/polymer overlap over a z-length of 3.8 ± 0.4 Å at the onset of the interfacial region (value obtained from an average of five independent MD simulations, with an error bar given by the standard deviation). For comparison, the composite constructed with a rigid MOF model led to a similar density plot (Figure S6) and comparable MOF/polymer overlap dimensions (3.4 ± 0.4 Å). The average length of *region A* in the z-axis was found to be 6 ± 2 Å and 5 ± 1 Å for the flexible- and rigid- MOF/Polymer composite models, respectively. This shows that PIM-1's packing efficiency does not depend on the NUS-8 surface flexibility, suggesting that it is instead controlled by its intrinsically rigid molecular ladder configuration. Relevant site-to-site radial distribution functions (RDFs) between the two components were further computed from the MD simulations (Figure S7). The most prominent MOF/Polymer interaction at the interface involves the cyano groups of PIM-1 and the hydroxyl groups of NUS-8 with a characteristic N_{PIM-1}...H_{NUS-8} distance of 2.6 Å as shown in Figure 1c. Analyses of the pore size distribution (PSD) of the
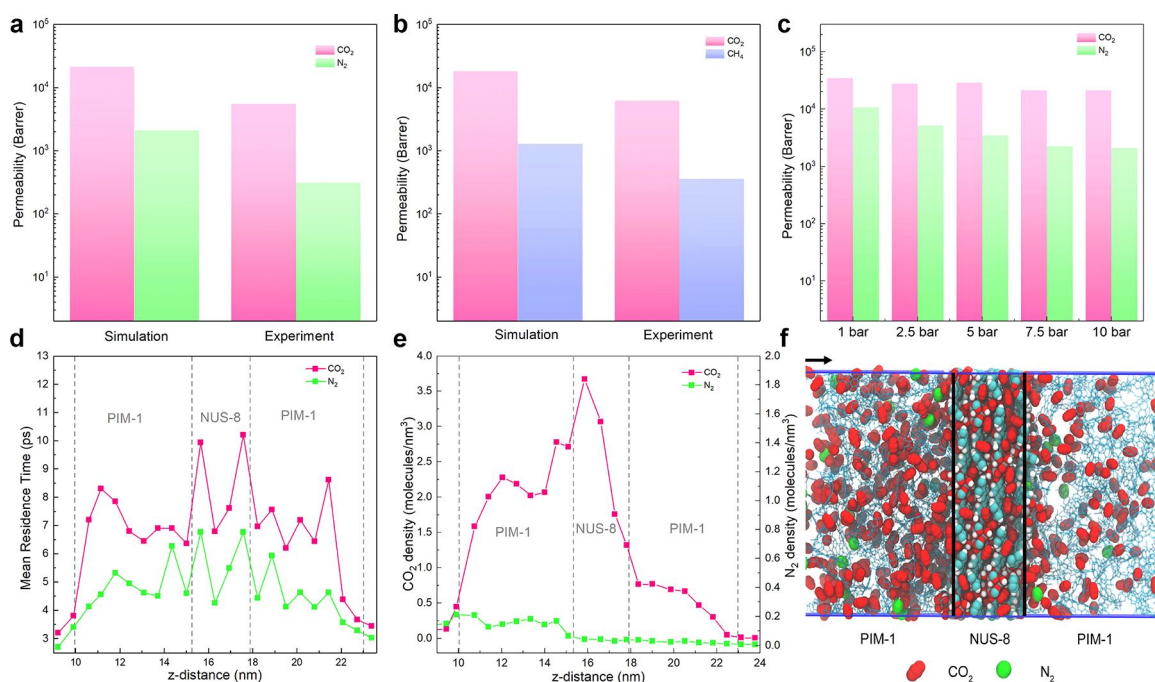
Figure 3. Gas mixture transport properties of the NUS-8/PIM-1 composite. (a, b) Simulated (at 10 bar feed) and experimental[29] gas permeabilities for equimolar CO_2/N_2 and CO_2/CH_4 mixtures, respectively. (c) Evolution of the simulated gas permeabilities as a function of the total feed pressure for the CO_2/N_2 mixture. (d) Mean residence time profiles for CO_2 and N_2 along the NUS-8/PIM-1 composite for an equimolar CO_2/N_2 mixture at 10 bar feed. Dashed lines indicate the average position of the NUS-8 and PIM-1 components. (e) Density profiles for CO_2 and N_2 along the NUS-8/PIM-1 composite for an equimolar CO_2/N_2 mixture at 10 bar feed. (f) Illustration of the typical distribution of CO_2 and N_2 molecules along the composite for an equimolar CO_2/N_2 mixture at 10 bar feed. Color scheme: PIM-1, blue wireframe; O, red; C (NUS-8), cyan. The arrow on the top left margin points to the direction of the gas flux.

whole composite revealed that the NUS-8 nanosheet and polymer regions exhibit pores of about 5.4 Å and up to 8.5 Å respectively (see Figures S5 and S8) reminiscent of what was previously obtained for the pure bulk NUS-8[32] and PIM-1.[31] Interestingly, as illustrated in the zoomed-in image of Figure 1a, relatively large voids, with diameters up to 11 Å, are created at the interface. These newly generated interfacial microvoids are expected to control the thermodynamics and dynamics of the gas adsorption/separation properties of the composite.

GCMC simulations were further performed to explore the gas adsorption properties of the NUS-8/PIM-1 composite model at 298 K. As a preliminary step, the atomistic models for both NUS-8, PIM-1, and the three guests CO_2, N_2, and CH_4 were validated by a good agreement between the simulated single-component adsorption isotherms for both individual MOF and polymer and the corresponding experimental data (see Figures S9–S14). Figure 2a shows the excellent agreement between the GCMC-simulated and experimentally obtained single-component N_2, CO_2, and CH_4 adsorption isotherms for the composite. This demonstrates that our atomistic model faithfully represents the NUS-8/PIM-1 composite. We further explored the thermodynamic separation performances of the composite with respect to the equimolar CO_2/CH_4 and CO_2/N_2 mixtures. The simulated coadsorption isotherms reported in Figure S15 highlight that the composite preferentially adsorbs CO_2 over both CH_4 and N_2, which is consistent with the higher CO_2 adsorption enthalpy calculated for the single components (CO_2: 39.3 kJ mol^{-1}, CH_4: 14.6 kJ mol^{-1}, and N_2: 10.9 kJ mol^{-1}). Figure 2b shows the simulated CO_2/CH_4 and CO_2/N_2 selectivities along with the gas uptakes at 1 bar for the composite as well as for the pure NUS-8 and PIM-1 models. These calculations reveal a slight increase of

both CO_2/N_2 and CO_2/CH_4 thermodynamic selectivity for the NUS-8/PIM-1 composite at 1 bar as compared with the pure PIM-1 from 26 to 29 and from 12 to 13, respectively. This is consistent with previous experimental findings for these systems.[29] The microscopic origin of this high thermodynamic selectivity for CO_2 was further elucidated by a careful analysis of the coadsorption mechanism in the composite. CO_2 was shown to interact more strongly with the hydroxyl group present at the NUS-8 surface and the oxygen atom of PIM-1, with characteristic $O_{CO_2}-H_{NUS-8}(OH)$ and $C_{CO_2}-O_{PIM-1}$ distances of 2.8 and 3.4 Å, respectively, as revealed by the corresponding RDFs plots and illustrative snapshots (Figure 2c). Figure 2d shows the number of gas molecules as a function of the z coordinate, along with an illustration for the CO_2/N_2 case at 1 bar. It can be deduced that both molecules can occupy all the different regions within the composite, with a more predominant CO_2 population compared to N_2. Note that CO_2 preferentially concentrates at *region A* of the NUS-8/PIM-1 composite as illustrated in Figure 2d. This scenario is explained by the interactions between CO_2 and the hydroxyl groups at the NUS-8 surface as discussed above, since these groups are exposed to the microvoids present in *region A*. A similar profile was also found for the CO_2/CH_4 mixture (Figure S17).

As a further step, CGD-MD simulations[30] were conducted at 298 K in order to gain insight into the transport properties of CO_2, N_2, and CH_4 through the MOF/polymer composite. For these simulations, we considered a larger and unwrapped composite model with dimensions of 40.39 × 70.10 × 129.80 Å^3, generated by placing a NUS-8 surface between two unwrapped PIM-1 slabs taken from our previously detailed

interface model. A typical snapshot of the simulation box is illustrated in Figure S18. Initially, the gas permeabilities were simulated for the equimolar CO_2/N_2 and CO_2/CH_4 mixtures at a total feed pressure of 10 bar and compared with the corresponding experimental data as reported in panels a and b, respectively, of Figure 3. We verified that the total pressure was maintained fixed at the target values over the simulation time (see Figure S19) and that 100 ns is enough to reach the steady state in our model system (see Figure S20a). A good agreement between the predicted permeabilities and the averaged available experimental values was obtained for the three gases in this composite. Note that similar NEMD studies usually lead to calculated permeabilities within an order of magnitude of the experimental ones.[43−45] The relative overprediction of the permeability is in line with the high permeation for the ultrathin membrane limit reported in the literature,[46−48] since our calculations were performed using an ultrathin NUS-8/PIM-1 composite model (∼13 nm along z-direction). The gas permeabilities for the CO_2/N_2 mixture were equally explored as a function of the feed gas pressure, with the permeate side of the composite set to vacuum. The drop in permeability with respect to increasing pressure in glassy polymeric membranes as well as in microporous carbon membranes[49] is a well-known phenomenon.[6,50,51] Interestingly, our NEMD calculations performed on the NUS-8/PIM-1 composite model capture this experimentally observed permeation trend.

Moreover, our predicted permeation selectivities for CO_2/CH_4 (16) and CO_2/N_2 (11) mixtures reproduce the experimental trend, with values in the range of 18−30 and 15−25 respectively. Altogether, this shows the reliability of the GCD-MD approach applied to a realistic atomistic model of the MOF/polymer composite to provide a fair prediction of its transport properties. As a further step, we explored the microscopic gas transport mechanism at the origin of the CO_2/N_2 and CO_2/CH_4 permeation selectivity in this MMM. Figure 3d,e report the mean residence time and steady-state concentration profiles, respectively, for CO_2 and N_2 in the binary mixture along the z-direction of the composite at 10 bar. Dashed lines are given to indicate the average position of the polymer and MOF components to guide the reader's eye, note that these positions fluctuate along the simulation. The residence time and steady-state concentration profiles can be considered respectively as the microscopic counterparts of the diffusion and solubility contributions of each penetrant's permeability in the scheme of solution-diffusion theory.[50,51] It turns out that while CO_2 and N_2 show rather similar residence time distributions in the whole composite (Figure 3d), a much more pronounced difference is observed between the two gases in the steady-state concentration profiles (Figure 3e). Indeed, the solubility contribution to selectivity is on average 23 times higher for CO_2 than for N_2, while the diffusion contribution for CO_2 is on average 0.7 of that for N_2. The corresponding solubility and diffusion selectivity values ratios are given in Figure S20b,c. This demonstrates that the solubility contribution dominates over the diffusion counterpart for the separation of the two gases in this composite and that this phenomenon is at the origin of the high CO_2/N_2 selectivity observed both experimentally and in our GCMC simulations. Similarly, solubility dominates the gas-separation process for the CO_2/CH_4 mixture as well, as shown by the corresponding residence times and steady-state concentration profiles given in the SI (Figure S21). Figure 3f reports a representative snapshot taken from our GCD-MD simulations to visually track the adsorbed CO_2 molecules through the composite model. This distribution of gas molecules is maintained along the simulation time, as the voids present in the interfacial region remain of similar size (11 Å) along the whole CGD-MD trajectories for the CO_2/N_2 mixture permeation (see Figure S22). Additional calculations were performed for the CO_2/N_2 gas mixture on pure NUS-8 and PIM-1 membrane models (see Figure S18 and Table S7). Interestingly, we demonstrated that the CO_2/N_2 selectivity of the MMM is not adversely affected by the presence of voids at the MOF/polymer interface since the selectivity of the NUS-8/PIM-1 composite is predicted to match that for the NUS-8 pure membrane (Table S7).

In a nutshell, our simulations suggest that the high CO_2 separation ability of the NUS-8/PIM-1 MMM can be explained via a solubility dominated separation mechanism and a favorable CO_2 adsorption through the emergent interfacial porosity. This predicted trend is in line with what has been previously evoked by an experimental study[52] on a silica-polyimide MMM system. In that study, the authors assumed that the presence of voids is the main reason behind the increase in the gas permeability of their MMM, as compared with its individual components. In a previous computational study, we reported that ZIF-8/PIM-1 MMMs show a reduced CH_4/H_2 separation ability as compared with its individual components because of the existence of voids at the interface which were at the origin of a loss of selectivity performance.[28] In this later case, the diffusion dominated the separation process because of the considerable effective size difference between CH_4 and H_2 molecules. The simultaneous consideration of these two different cases demonstrates that the presence of interfacial void regions can have either a positive or a negative impact into the separation performance of the MMM, depending on whether the separation mechanism is governed by solubility or by diffusion, respectively. It could be speculated that both a rigid polymer,that promotes the formation of microvoids at the MOF/polymer interface, together with a MOF surface decorated by chemical functions with high CO_2 affinity, might contribute to a solubility driven mechanism for CO_2 pre- and post-combustion separations. In the future, we plan to scan several MOF/polymer composites in order to explore the validity of this hypothesis.

In summary, the impact of the MOF/polymer interface into the thermodynamics and dynamics of CO_2/N_2 and CO_2/CH_4 separation properties of a model NUS-8/PIM-1 MMM was explored by means of molecular simulations. Our approach integrated DFT calculations with GCMC, MD, and CGD-MD simulations, thus enabling us to go all the way from building a realistic composite model at the atomistic level, to exploring the adsorption and the transport mechanism of the gas mixtures. We have found that there are microvoids at the NUS-8/PIM-1 interface and that the CO_2 molecules are preferentially adsorbed at these microvoids thanks to its strong interactions with the hydroxyl groups at the NUS-8 surface. The presence of this interfacial porosity does not adversely affect the MMM separation performance thanks to a solubility-driven separation mechanism. Previous studies have considered the CH_4/H_2 separation in ZIF-8/PIM-1 composites and found that the interfacial porosity was detrimental to the separation performances of the composite with respect to pure PIM-1, which can be ascribed to a diffusion-driven separation

mechanism. By considering both the previous and our current results, it can be concluded that the separation mechanism needs to be taken into account in order to determine whether the separation abilities of the MMM will deteriorate or not in the presence of interfacial porosities, contrary to the regular belief that porosity is always detrimental to separation performance. We believe that these results will help gas-separation membranes development by shifting the focus to new strategies that rely on solubility-driven separations.

■ ASSOCIATED CONTENT

ⓈⒾ Supporting Information

The Supporting Information is available free of charge at https://pubs.acs.org/doi/10.1021/acsmaterialslett.0c00560.

> Force fields, models derivation, calculation setup details, and additional validation/results plots (PDF)

■ AUTHOR INFORMATION

Corresponding Author

Rocio Semino − *ICGM, Univ. Montpellier, CNRS, ENSCM, Montpellier, France;* ⓞ orcid.org/0000-0003-3937-7414; Email: rocio.semino@umontpellier.fr

Authors

Dong Fan − *ICGM, Univ. Montpellier, CNRS, ENSCM, Montpellier, France;* ⓞ orcid.org/0000-0003-1873-3416

Aydin Ozcan − *ICGM, Univ. Montpellier, CNRS, ENSCM, Montpellier, France*

Naseem A. Ramsahye − *ICGM, Univ. Montpellier, CNRS, ENSCM, Montpellier, France*

Dan Zhao − *Department of Chemical and Biomolecular Engineering, National University of Singapore, Singapore 117585;* ⓞ orcid.org/0000-0002-4427-2150

Guillaume Maurin − *ICGM, Univ. Montpellier, CNRS, ENSCM, Montpellier, France;* ⓞ orcid.org/0000-0002-2096-0450

Complete contact information is available at:
https://pubs.acs.org/10.1021/acsmaterialslett.0c00560

Author Contributions

§(D.F., A.O.) These authors contributed equally.

Notes

The authors declare no competing financial interest.

■ ACKNOWLEDGMENTS

■ REFERENCES

(1) Park, H. B.; Kamcev, J.; Robeson, L. M.; Elimelech, M.; Freeman, B. D. Maximizing the Right Stuff: The Trade-off between Membrane Permeability and Selectivity. *Science* **2017**, *356*, eaab0530.

(2) Koros, W. J.; Fleming, G. K. Membrane-Based Gas Separation. *J. Membr. Sci.* **1993**, *83*, 1−80.

(3) Castro-Muñoz, R.; Agrawal, K. V.; Coronas, J. Ultrathin Permselective Membranes: The Latent Way for Efficient Gas Separation. *RSC Adv.* **2020**, *10*, 12653−12670.

(4) Seoane, B.; Coronas, J.; Gascon, I.; Benavides, M. E.; Karvan, O.; Caro, J.; Kapteijn, F.; Gascon, J. Metal−Organic Framework Based Mixed Matrix Membranes: A Solution for Highly Efficient CO_2 Capture? *Chem. Soc. Rev.* **2015**, *44*, 2421−2454.

(5) Galizia, M.; Chi, W. S.; Smith, Z. P.; Merkel, T. C.; Baker, R. W.; Freeman, B. D. *50th Anniversary Perspective*: Polymers and Mixed Matrix Membranes for Gas and Vapor Separation: A Review and Prospective Opportunities. *Macromolecules* **2017**, *50*, 7809−7843.

(6) Qian, Q.; Asinger, P. A.; Lee, M. J.; Han, G.; Mizrahi Rodriguez, K.; Lin, S.; Benedetti, F. M.; Wu, A. X.; Chi, W. S.; Smith, Z. P. MOF-Based Membranes for Gas Separations. *Chem. Rev.* **2020**, *120*, 8161−8266.

(7) Koros, W. J.; Zhang, C. Materials for Next-Generation Molecularly Selective Synthetic Membranes. *Nat. Mater.* **2017**, *16*, 289−297.

(8) Liu, G.; Chernikova, V.; Liu, Y.; Zhang, K.; Belmabkhout, Y.; Shekhah, O.; Zhang, C.; Yi, S.; Eddaoudi, M.; Koros, W. J. Mixed Matrix Formulations with MOF Molecular Sieving for Key Energy-Intensive Separations. *Nat. Mater.* **2018**, *17*, 283−289.

(9) Rodenas, T.; Luz, I.; Prieto, G.; Seoane, B.; Miro, H.; Corma, A.; Kapteijn, F.; Llabrés i Xamena, F. X.; Gascon, J. Metal−Organic Framework Nanosheets in Polymer Composite Materials for Gas Separation. *Nat. Mater.* **2015**, *14*, 48−55.

(10) Kalaj, M.; Bentz, K. C.; Ayala, S.; Palomba, J. M.; Barcus, K. S.; Katayama, Y.; Cohen, S. M. MOF-Polymer Hybrid Materials: From Simple Composites to Tailored Architectures. *Chem. Rev.* **2020**, *120*, 8267−8302.

(11) Cheng, Y.; Wang, X.; Jia, C.; Wang, Y.; Zhai, L.; Wang, Q.; Zhao, D. Ultrathin Mixed Matrix Membranes Containing Two-Dimensional Metal-Organic Framework Nanosheets for Efficient CO_2/CH_4 Separation. *J. Membr. Sci.* **2017**, *539*, 213−223.

(12) Knebel, A.; Bavykina, A.; Datta, S. J.; Sundermann, L.; Garzon-Tovar, L.; Lebedev, Y.; Durini, S.; Ahmad, R.; Kozlov, S. M.; Shterk, G.; Karunakaran, M.; Carja, I. D.; Simic, I. D.; Weilert, I.; Klüppel, M.; Giese, U.; Cavallo, L.; Rueping, M.; Eddaoudi, M.; Caro, J.; Gascon, J. Solution Processable Metal−Organic Frameworks for Mixed Matrix Membranes Using Porous Liquids. *Nat. Mater.* **2020**, *19*, 1346−1353.

(13) Pustovarenko, A.; Goesten, M. G.; Sachdeva, S.; Shan, M.; Amghouz, Z.; Belmabkhout, Y.; Dikhtiarenko, A.; Rodenas, T.; Keskin, D.; Voets, I. K.; Weckhuysen, B. M.; Eddaoudi, M.; de Smet, L. C. P. M.; Sudhölter, E. J. R.; Kapteijn, F.; Seoane, B.; Gascon, J. Nanosheets of Nonlayered Aluminum Metal-Organic Frameworks through a Surfactant-Assisted Method. *Adv. Mater.* **2018**, *30*, 1707234.

(14) Denny, M. S.; Cohen, S. M. In Situ Modification of Metal-Organic Frameworks in Mixed-Matrix Membranes. *Angew. Chem., Int. Ed.* **2015**, *54*, 9029−9032.

(15) Troyano, J.; Carné-Sánchez, A.; Pérez-Carvajal, J.; León-Reina, L.; Imaz, I.; Cabeza, A.; Maspoch, D. A Self-Folding Polymer Film Based on Swelling Metal−Organic Frameworks. *Angew. Chem.* **2018**, *130*, 15646−15650.

(16) Wang, H.; He, S.; Qin, X.; Li, C.; Li, T. Interfacial Engineering in Metal−Organic Framework-Based Mixed Matrix Membranes Using Covalently Grafted Polyimide Brushes. *J. Am. Chem. Soc.* **2018**, *140*, 17203−17210.

(17) Barankova, E.; Tan, X.; Villalobos, L. F.; Litwiller, E.; Peinemann, K.-V. A Metal Chelating Porous Polymeric Support: The Missing Link for a Defect-Free Metal-Organic Framework Composite Membrane. *Angew. Chem., Int. Ed.* **2017**, *56*, 2965−2968.

(18) Liu, Y.; Liu, G.; Zhang, C.; Qiu, W.; Yi, S.; Chernikova, V.; Chen, Z.; Belmabkhout, Y.; Shekhah, O.; Eddaoudi, M.; Koros, W. Enhanced CO_2/CH_4 Separation Performance of a Mixed Matrix Membrane Based on Tailored MOF-Polymer Formulations. *Adv. Sci.* **2018**, *5*, 1800982.

(19) Hao, L.; Liao, K.-S.; Chung, T.-S. Photo-Oxidative PIM-1 Based Mixed Matrix Membranes with Superior Gas Separation Performance. *J. Mater. Chem. A* **2015**, *3*, 17273−17281.

(20) Semino, R.; Moreton, J. C.; Ramsahye, N. A.; Cohen, S. M.; Maurin, G. Understanding the Origins of Metal−Organic Framework/Polymer Compatibility. *Chem. Sci.* **2018**, *9*, 315−324.

(21) Tavares, S. R.; Ramsahye, N. A.; Adil, K.; Eddaoudi, M.; Maurin, G.; Semino, R. Computationally Assisted Assessment of the Metal-Organic Framework/Polymer Compatibility in Composites Integrating a Rigid Polymer. *Adv. Theory Simul.* **2019**, *2*, 1900116.

(22) Moore, T. T.; Koros, W. J. Non-Ideal Effects in Organic−Inorganic Materials for Gas Separation Membranes. *J. Mol. Struct.* **2005**, *739*, 87−98.

(23) Hillock, A. M. W.; Miller, S. J.; Koros, W. J. Crosslinked Mixed Matrix Membranes for the Purification of Natural Gas: Effects of Sieve Surface Modification. *J. Membr. Sci.* **2008**, *314*, 193−199.

(24) Duan, P.; Moreton, J. C.; Tavares, S. R.; Semino, R.; Maurin, G.; Cohen, S. M.; Schmidt-Rohr, K. Polymer Infiltration into Metal−Organic Frameworks in Mixed-Matrix Membranes Detected in Situ by NMR. *J. Am. Chem. Soc.* **2019**, *141*, 7589−7595.

(25) Vinh-Thang, H.; Kaliaguine, S. Predictive Models for Mixed-Matrix Membrane Performance: A Review. *Chem. Rev.* **2013**, *113*, 4980−5028.

(26) Zhang, L.; Hu, Z.; Jiang, J. Metal−Organic Framework/Polymer Mixed-Matrix Membranes for H_2/CO_2 Separation: A Fully Atomistic Simulation Study. *J. Phys. Chem. C* **2012**, *116*, 19268−19277.

(27) Dutta, R. C.; Bhatia, S. K. Interfacial Engineering of MOF-Based Mixed Matrix Membrane through Atomistic Simulations. *J. Phys. Chem. C* **2020**, *124*, 594−604.

(28) Ozcan, A.; Semino, R.; Maurin, G.; Yazaydin, A. O. Modeling of Gas Transport through Polymer/MOF Interfaces: A Microsecond-Scale Concentration Gradient-Driven Molecular Dynamics Study. *Chem. Mater.* **2020**, *32*, 1288−1296.

(29) Cheng, Y.; Tavares, S. R.; Doherty, C. M.; Ying, Y.; Sarnello, E.; Maurin, G.; Hill, M. R.; Li, T.; Zhao, D. Enhanced Polymer Crystallinity in Mixed-Matrix Membranes Induced by Metal−Organic Framework Nanosheets for Efficient CO_2 Capture. *ACS Appl. Mater. Interfaces* **2018**, *10*, 43095−43103.

(30) Ozcan, A.; Perego, C.; Salvalaglio, M.; Parrinello, M.; Yazaydin, O. Concentration Gradient Driven Molecular Dynamics: A New Method for Simulations of Membrane Permeation and Separation. *Chem. Sci.* **2017**, *8*, 3858−3865.

(31) Semino, R.; Ramsahye, N. A.; Ghoufi, A.; Maurin, G. Microscopic Model of the Metal−Organic Framework/Polymer Interface: A First Step toward Understanding the Compatibility in Mixed Matrix Membranes. *ACS Appl. Mater. Interfaces* **2016**, *8*, 809−819.

(32) Hu, Z.; Mahdi, E. M.; Peng, Y.; Qian, Y.; Zhang, B.; Yan, N.; Yuan, D.; Tan, J.-C.; Zhao, D. Kinetically Controlled Synthesis of Two-Dimensional Zr/Hf Metal−Organic Framework Nanosheets via a Modulated Hydrothermal Approach. *J. Mater. Chem. A* **2017**, *5*, 8954−8963.

(33) Hutter, J.; Iannuzzi, M.; Schiffmann, F.; VandeVondele, J. CP2K: Atomistic Simulations of Condensed Matter Systems. *WIREs Comput. Mol. Sci.* **2014**, *4*, 15−25.

(34) Kühne, T. D.; Iannuzzi, M.; Del Ben, M.; Rybkin, V. V.; Seewald, P.; Stein, F.; Laino, T.; Khaliullin, R. Z.; Schütt, O.; Schiffmann, F.; Golze, D.; Wilhelm, J.; Chulkov, S.; Bani-Hashemian, M. H.; Weber, V.; Borštnik, U.; Taillefumier, M.; Jakobovits, A. S.; Lazzaro, A.; Pabst, H.; Müller, T.; Schade, R.; Guidon, M.; Andermatt, S.; Holmberg, N.; Schenter, G. K.; Hehn, A.; Bussy, A.; Belleflamme, F.; Tabacchi, G.; Glöß, A.; Lass, M.; Bethune, I.; Mundy, C. J.; Plessl, C.; Watkins, M.; VandeVondele, J.; Krack, M.; Hutter, J. CP2K: An Electronic Structure and Molecular Dynamics Software Package - Quickstep: Efficient and Accurate Electronic Structure Calculations. *J. Chem. Phys.* **2020**, *152*, 194103.

(35) Abbott, L. J.; Hart, K. E.; Colina, C. M. Polymatic: A Generalized Simulated Polymerization Algorithm for Amorphous Polymers. *Theor. Chem. Acc.* **2013**, *132*, 1334.

(36) Todorov, I. T.; Smith, W.; Trachenko, K.; Dove, M. T. DL_POLY_3: New Dimensions in Molecular Dynamics Simulations via Massive Parallelism. *J. Mater. Chem.* **2006**, *16*, 1911.

(37) Rappe, A. K.; Casewit, C. J.; Colwell, K. S.; Goddard, W. A.; Skiff, W. M. UFF, a Full Periodic Table Force Field for Molecular Mechanics and Molecular Dynamics Simulations. *J. Am. Chem. Soc.* **1992**, *114*, 10024−10035.

(38) Wang, J.; Wolf, R. M.; Caldwell, J. W.; Kollman, P. A.; Case, D. A. Development and Testing of a General Amber Force Field. *J. Comput. Chem.* **2004**, *25*, 1157−1174.

(39) Potoff, J. J.; Siepmann, J. I. Vapor−Liquid Equilibria of Mixtures Containing Alkanes, Carbon Dioxide, and Nitrogen. *AIChE J.* **2001**, *47*, 1676−1682.

(40) Dubbeldam, D.; Calero, S.; Ellis, D. E.; Snurr, R. Q. RASPA: Molecular Simulation Software for Adsorption and Diffusion in Flexible Nanoporous Materials. *Mol. Simul.* **2016**, *42*, 81−101.

(41) Abraham, M. J.; Murtola, T.; Schulz, R.; Páll, S.; Smith, J. C.; Hess, B.; Lindahl, E. GROMACS: High Performance Molecular Simulations through Multi-Level Parallelism from Laptops to Supercomputers. *SoftwareX* **2015**, *1*, 19−25.

(42) Tribello, G. A.; Bonomi, M.; Branduardi, D.; Camilloni, C.; Bussi, G. PLUMED 2: New Feathers for an Old Bird. *Comput. Phys. Commun.* **2014**, *185*, 604−613.

(43) Frentrup, H.; Hart, K.; Colina, C.; Muller, E. In Silico Determination of Gas Permeabilities by Non-Equilibrium Molecular Dynamics: CO_2 and He through PIM-1. *Membranes* **2015**, *5*, 99−119.

(44) Zhang, Y.; Furukawa, S.-I.; Nitta, T. Computer Simulation Studies on Gas Permeation of Propane and Propylene across ZSM-5 Membranes by a Non-Equilibrium Molecular Dynamics Technique. *Sep. Purif. Technol.* **2003**, *32*, 215−221.

(45) Kobayashi, Y.; Takami, S.; Kubo, M.; Miyamoto, A. Non-Equilibrium Molecular Simulation Studies on Gas Separation by Microporous Membranes Using Dual Ensemble Molecular Simulation Techniques. *Fluid Phase Equilib.* **2002**, *194*, 319−326.

(46) Li, W.; Su, P.; Li, Z.; Xu, Z.; Wang, F.; Ou, H.; Zhang, J.; Zhang, G.; Zeng, E. Ultrathin Metal−Organic Framework Membrane Production by Gel−Vapour Deposition. *Nat. Commun.* **2017**, *8*, 406.

(47) Lee, M. J.; Abdul Hamid, M. R.; Lee, J.; Kim, J. S.; Lee, Y. M.; Jeong, H.-K. Ultrathin Zeolitic-Imidazolate Framework ZIF-8 Membranes on Polymeric Hollow Fibers for Propylene/Propane Separation. *J. Membr. Sci.* **2018**, *559*, 28−34.

(48) Wei, R.; Chi, H.; Li, X.; Lu, D.; Wan, Y.; Yang, C.; Lai, Z. Aqueously Cathodic Deposition of ZIF-8 Membranes for Superior Propylene/Propane Separation. *Adv. Funct. Mater.* **2020**, *30*, 1907089.

(49) Boţan, A.; Vermorel, R.; Ulm, F.-J.; Pellenq, R. J.-M. Molecular Simulations of Supercritical Fluid Permeation through Disordered Microporous Carbons. *Langmuir* **2013**, *29*, 9985−9990.

(50) Drioli, E.; Giorno, L. *Encyclopedia of Membranes*; Springer, 2018.

(51) Freeman, B.; Yampolskii, Y.; Pinnau, I. *Materials Science of Membranes for Gas and Vapor Separation*; John Wiley & Sons, 2006.

(52) Cornelius, C. J.; Marand, E. Hybrid Silica-Polyimide Composite Membranes: Gas Transport Properties. *J. Membr. Sci.* **2002**, *202*, 97−118.